

CHANGES IN GLOTTAL AREA ASSOCIATED WITH INCREASING AIRFLOW

JOEL A. SERCARZ, MD

LOS ANGELES, CALIFORNIA

JODY KREIMAN, PHD

LOS ANGELES, CALIFORNIA

GERALD S. BERKE, MD

LOS ANGELES, CALIFORNIA

MING YE, MD

LOS ANGELES, CALIFORNIA

STEVEN BIELAMOWICZ, MD

LOS ANGELES, CALIFORNIA

DAVID C. GREEN, MD

SEATTLE, WASHINGTON

Laryngeal resistance varies inversely with airflow during phonation. This study evaluated the morphological changes in the glottis that accompany decreases in laryngeal resistance at higher levels of airflow. An *in vivo* canine model of phonation and a video analysis system were used to assess changes in area. Four animals were examined stroboscopically as airflow increased, with constant recurrent laryngeal nerve stimulation. Glottal dynamics were evaluated by means of photoglottography, electroglottography, and measures of subglottic pressure. Analysis of digitized stroboscopic images indicated that increasing airflow had no obvious effect on the glottal chink (vocal process contact). Increasing airflow was associated with an increase in the area of peak opening and an increase in the glottal area integral.

KEY WORDS — airflow, glottal area, laryngeal resistance, larynx, phonation.

INTRODUCTION

Laryngeal resistance is defined as mean subglottic pressure divided by mean airflow rate.¹ The decrease in laryngeal resistance occurring at higher airflow has two possible explanations. First, the duration or frequency of laryngeal opening may increase with increasing airflow. Alternatively, examination of serial videostroboscopic images suggests that the decrease in laryngeal resistance may be due to increases in glottal area with increasing flow. Analysis of electroglottography (EGG) waveforms has shown that the open quotient (defined as the duration of glottal opening divided by the duration of the cycle) increases with airflow.² Glottal area at various levels of airflow has not been measured directly.

The present study uses techniques developed recently in our laboratory to quantify morphological features of the vibrating larynx, including glottal area, from videostroboscopic images.³ Glottal area integral over one cycle of phonation can be calculated from these measures by synchronizing the videostroboscopic images with EGG waveforms and then plotting area versus time. These techniques allow measurement of the effect of changes in airflow on the morphology of the vibrating larynx. Without such *in vivo* measurements, the relationship between glottal geometry and airflow has been limited to theoretic discussion.

MATERIALS AND METHODS

In Vivo Canine Model. The *in vivo* canine model of

phonation is depicted in Fig 1, and has been described in detail in previous reports.⁴ Four mongrel dogs (approximately 20 kg each) were premedicated with acepromazine maleate intramuscularly. Intravenous thiopental sodium was administered to a level of corneal anesthesia. Additional thiopental sodium was

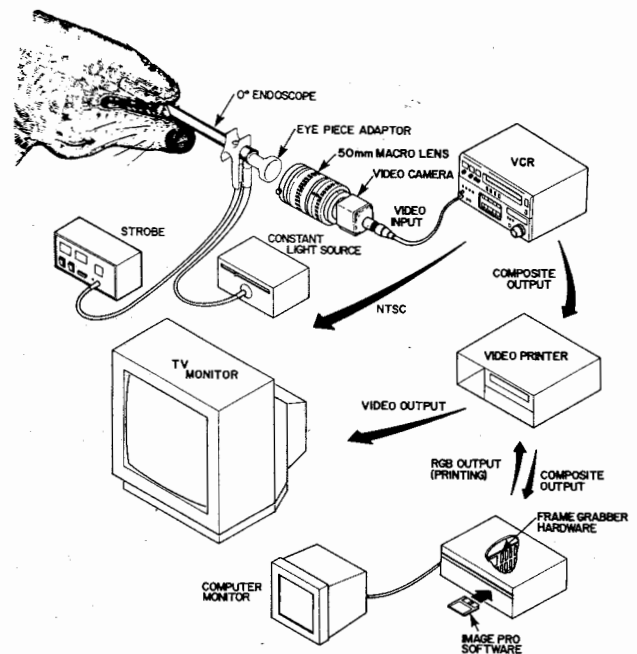


Fig 1. System used for measurement of videostroboscopic images in *in vivo* canine model of phonation. NTSC — National Television Standards Commission, RGB — red, green, blue.

From the Division of Head and Neck Surgery, University of California, Los Angeles, California. Supported by the American Laryngological Association Research Award. This study was performed in accordance with the PHS Policy on Humane Care and Use of Laboratory Animals, the NIH Guide for the Care and Use of Laboratory Animals, and the Animal Welfare Act (7 U.S.C. et seq.); the animal use protocol was approved by the Institutional Animal Care and Use Committee (IACUC) of the University of California, Los Angeles.



Fig 2. Centimeter ruler lowered to level of glottis and measured in pixels to allow conversion from pixels to square millimeters.

used to maintain this level of anesthesia throughout the procedure.

Animals were placed supine on the operating table. A midline incision was made to expose the trachea from the hyoid bone to the sternal notch. A low tracheostomy was performed at the level of the suprasternal notch and cannulated with an endotracheal tube for ventilation. A second tracheostomy was performed superiorly and a cuffed endotracheal tube was passed in a rostral direction with the tip positioned approximately 10 cm below the vocal folds. The cuff was inflated and air was passed through this rostral endotracheal tube from a laboratory wall outlet. The airflow was humidified and heated by bubbling it through 5 cm of heated water so that the temperature of the air was 37°C when measured at the glottal outlet.

Upstream subglottic pressure was measured with a catheter-tipped pressure transducer (model SPC-330; Millar Instruments, Houston, Tex). The subglottic pressure transducer was passed rostrally through the superior tracheostomy and placed 1 cm below the glottis.

Airflow was controlled by a valve at the laboratory wall outlet and measured with a flowmeter (model F1500; Gilmont Instruments, Great Neck, NY). One-centimeter segments of recurrent (RLN) and superior (SLN) laryngeal nerves were isolated and Harvard bipolar electrodes (South Natick, Mass) were ap-



Fig 3. Peak glottal area versus airflow.

plied. A constant current nerve stimulator (model S2LH; WR Medical Electronics Co, St Paul, Minn) was used to stimulate the RLNs, and a constant voltage source (model 54H; Grass Instruments, Quincy, Mass), was used to stimulate the SLNs. These nerves were stimulated at 70 to 80 Hz, with 0.3 to 0.5 mA (RLN) or 1 to 1.4 V (SLN) intensity for 1.5 milliseconds' pulse duration. Phonation was produced by discrete airflow intervals from 100 mL/s to 550 mL/s.

The photoglottography (PGG) and subglottic pressure signals were low-pass-filtered at 3 kHz, digitized at 20 kHz for 2.8 seconds, and stored on the hard disk of a personal computer.

Stroboscopy. Stroboscopic videoendoscopy was performed with a Karl Storz research stroboscope (model 8000, Culver City, Calif) used to illuminate the glottis through a 0° documentation sheath. Images were recorded with a charge-coupled device camera (model 70-5110; Jedmed, St Louis, Mo) and a 3/4-in professional videocassette recorder (model VO9850; Sony, Park Ridge, NJ).

Synchronization. The synchronization method used is described by Berke et al.⁵ A custom-made Kluge box produced a 5-millisecond square wave pulse (SWP). A Hitachi oscilloscope (model V-1050 F; Torrance, Calif) was used to separate the vertical synchronization trace of the video signal. Berke et al.⁵ showed previously that a SWP can be digitized and simultaneously recorded on the sound track of a videotape. A strobe flash is simultaneously recorded onto the PGG waveform, where it produces a sharp increase in the PGG signal. By recording both the SWP and the strobe flash, the timing of any stroboscopic image can be determined. By referring to the EGG waveform, the amount of time between the opening of the glottis and the recording of a given image can also be calculated.

Digitization. A Labmaster analog-to-digital microprocessor board housed in a personal computer

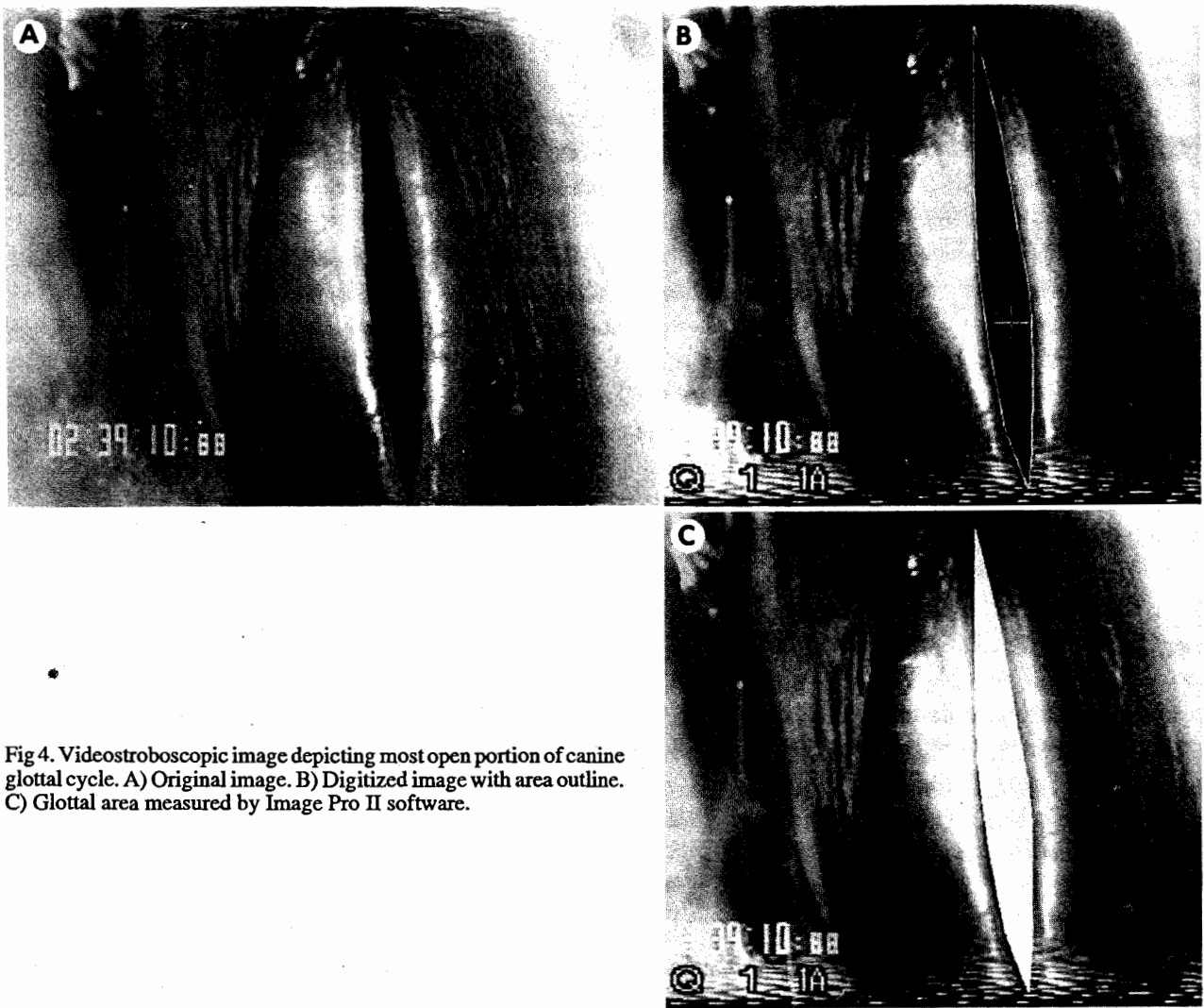


Fig 4. Videostroboscopic image depicting most open portion of canine glottal cycle. A) Original image. B) Digitized image with area outline. C) Glottal area measured by Image Pro II software.

with a math coprocessor allowed for four channels to be recorded: 1) EGG waveforms, 2) PGG waveforms, 3) SWP signals, and 4) the vertical trace of the video signals. The EGG and PGG signals were verified on a Tektronix oscilloscope (model 5116; Beaverton, Ore) before recording.

Videostroboscopic Image Evaluation. Glottal opening (area) was measured with a mouse-driven software package (Image Pro II, Media Cybernetics; Silver Spring, Md). The hardware necessary for area measurements in the dog is shown in Fig 1. The videostroboscopic image was first digitized by a Frame Grabber board (Data Translation, DT-2853 60SQ; Marlborough, Mass). After outlining of the desired portion of the digitized image, the area of the measured trace was expressed in pixel units by the software.

Figure 2 illustrates the calibration method used for an in vivo canine experiment. A standard centimeter ruler was lowered to the level of the glottis and

measured with the software, so that pixel units could be converted to square millimeters. The camera was kept at a constant distance from the larynx throughout each experiment.

Experimental Design. Three animals were studied by varying airflow from 100 to 550 mL/s at three to four discrete levels of flow. The peak area of each complete glottal cycle was calculated from 8 to 12 stroboscopic cycles. Each stroboscopic cycle lasted approximately 1 second and therefore represented several hundred cycles of vibration, depending on the frequency of phonation. The measures for each animal at each flow rate were averaged and the results plotted. The laryngeal nerve stimulation (RLN and SLN) was kept constant during the trials for each animal. To ensure that fatigue was not altering the results, the subglottic pressure was periodically assessed at a median flow rate (318 mL/s) and found to be constant.

One additional animal was studied to determine

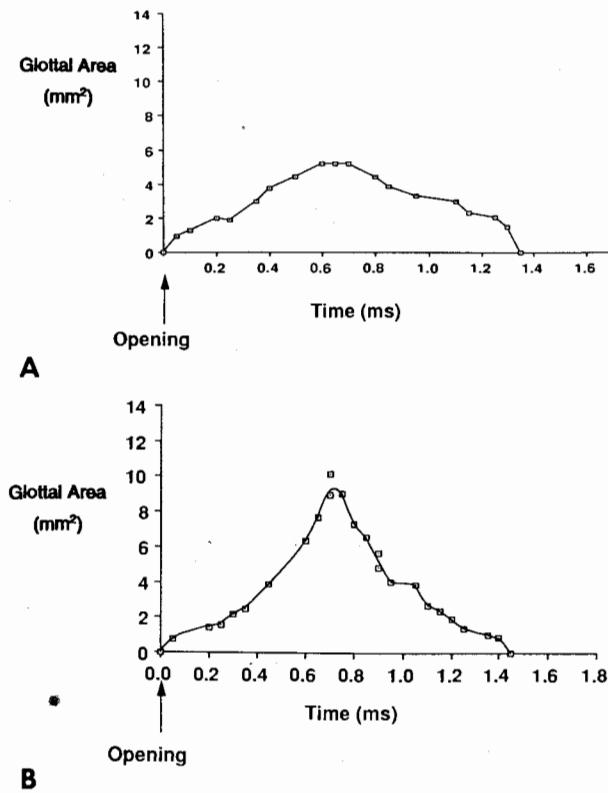
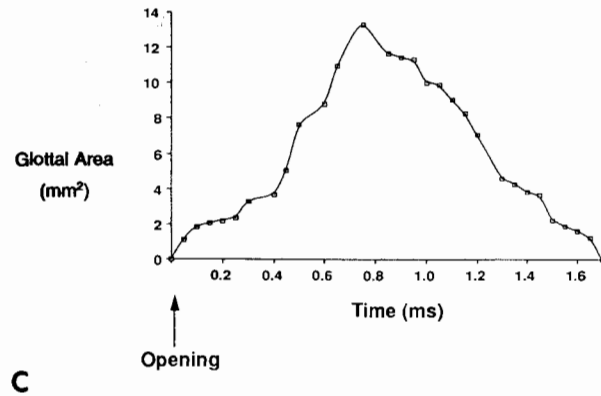


Fig 5. Effect of airflow on area for one glottal cycle. Nerve stimulation and subglottic pressure were kept constant across three trials with airflow at A) 150, B) 250, and C) 400 mL/s.



the integral of glottal area at three levels of flow. To determine the area for each point during the glottal cycle, the area of a series of images from one stroboscopic "cycle" was measured. The area was measured from each image and a graph relating area versus time was generated.

RESULTS

Because of individual variation in the simulated phonation in the animal subjects, peak area could not be measured at every level of flow for every dog. Consequently, dogs could not be combined in a single statistical analysis. However, a one-way analysis of variance (ANOVA) showed no significant overall differences among dogs in peak glottal areas across flow levels ($F_{2,8} = 1.400, p > .05$). Dogs were therefore combined for the following analysis.

Simple linear regression showed a significant and

substantial relationship between airflow and peak glottal area ($F_{1,9} = 71.36, p < .01; r^2 = .89$). This relationship is shown in Fig 3.

A sample videostroboscopic image of peak opening is shown in Fig 4A. Figure 4B,C shows the same image after digitization by the Frame Grabber hardware and measurement by the Image Pro software.

Figure 5 shows plots of the glottal area versus time waveforms from sequential glottographic images at three different airflow rates (150, 250, and 400 mL/s) in the same animal. Each area point represents one image from consecutive stroboscopic cycles. Time zero corresponds to the moment of opening of the upper vocal fold margins. The last point on each

DATA ANALYSIS OF FIGURE 5

Figure	Airflow (mL/s)	Peak Subglottic Pressure (mm Hg)	Area Integral (mm ² /s)	R ²	Frequency (Hz)
5A	150	24.9	3.99	.98	251
5B	250	23.8	5.48	.901	268
5C	400	24.9	10.19	.935	287

Fifth-order polynomial was generated for each curve and integrated to calculate area integral. R² is correlation coefficient of curve fit.

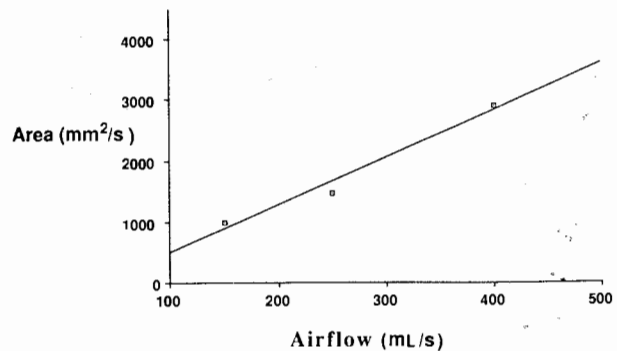


Fig 6. Product of area integral and fundamental frequency, versus three airflow rates (150, 250, and 400 mL/s). This measurement approximates "area per second."

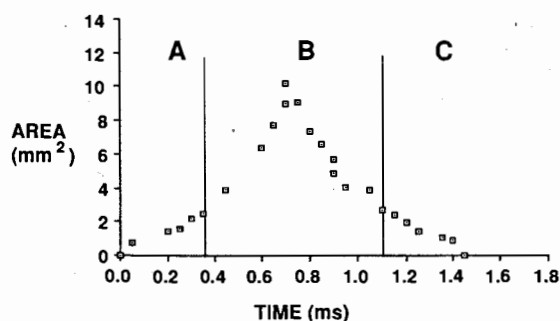


Fig 7. Events (laryngeal cycle) observed videostroboscopically corresponding to three portions of area waveform. A — upper margin unzipping, B — transverse displacement, C — “re-zipping” (lower margin). See text for discussion.

curve corresponds to the instant of closure of the lower folds. The timing of each image relative to laryngeal opening was determined by synchronizing the image to glottographic and subglottic pressure signals. A best-fit fifth-order polynomial was obtained for each glottal waveform by means of a commercial graphing software package (Cricket Graph; Garden City, NY). The mathematic equation was integrated to determine the area under the glottal area versus time waveform for one glottal cycle.

The glottal area integral, representing the cumulative glottal opening (area) during one glottal cycle, is outlined in the Table. Laryngeal nerve stimulation was kept constant during this experiment as the flow rate was altered. The integral was multiplied by the fundamental frequency in hertz to determine the glottal area per second of phonation in the model. This was plotted against airflow for three different flow rates in the same animal (Fig 6). This product increases with increasing airflow in a nearly linear fashion, although statistical analysis was not attempted because of the very small number of data points.

Analysis of the videostroboscopic data revealed no posterior glottal gap. In addition, no difference in interarytenoid distance was observed following changes in airflow.

DISCUSSION

Glottal area has previously been estimated by PGG, a measure of light passing through the glottal opening, and EGG, a measure of electrical impedance across the vocal folds. Quantitative measurements of glottal area have been made with high-speed photography, which is expensive and labor-intensive.⁶ This study provides direct measurements of glottal area through use of stroboscopic data and image analysis software.

The integral of the glottal area versus time wave-

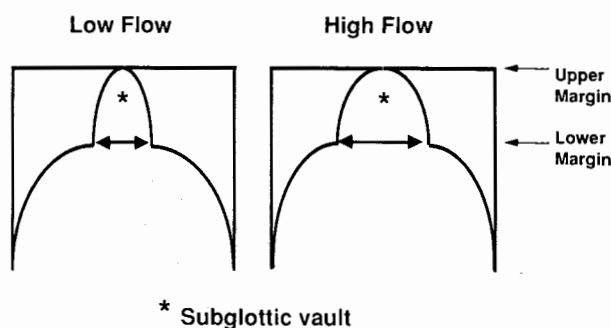


Fig 8. Proposed effect of airflow on subglottic vault. Higher airflow dilates subglottic vault, leading to greater area of opening.

form is the most meaningful method of examining the effect of airflow on glottal geometry. The glottal area integral evaluates both the duration and magnitude of opening, while an open quotient measures only the duration of opening, and the peak area assesses only the magnitude of glottal opening. Multiplying the area integral by the fundamental frequency provides a measure of the glottal area per second. This product increased with airflow in a nearly linear fashion (Fig 6). This relationship explains the decreases in laryngeal resistance that occur with increasing airflow.

The shapes of the glottal area versus time waveforms can be understood by analyzing the videostroboscopic sequences. In the first portion of the cycle (labeled A in Fig 7), glottal area increases slowly during unzipping of the upper margin of the vocal fold. During the middle portion of the cycle (labeled B), lateral displacement of the vocal cord occurs. This results in an abrupt increase in area. Finally, the lower margin of the vocal fold “re-zips,” causing flattening of the curve.

Peak area increased significantly with increased flow in the *in vivo* canine model. These findings are consistent with the canine study of Smith et al,² who analyzed glottal area from video screen tracings. Figure 8 shows one possible explanation for this finding. At higher airflow, a greater dilatation of the subglottic vault occurs before vocal fold opening. This increase in subglottic vault translates to increased excursion amplitude during vibration.

In these experiments increased airflow at the same level of nerve stimulation resulted in an increased area and therefore a decrease in glottal resistance. These conclusions were also reached by Smith et al² in 1991 and are consistent with Ohm's law for fluid systems. Figure 7 presents a possible explanation for the increase in area that occurs at greater airflow levels. The Figure shows the glottis at the moment before opening of the upper margins. With higher airflow, a greater dilatation of the subglottic vault

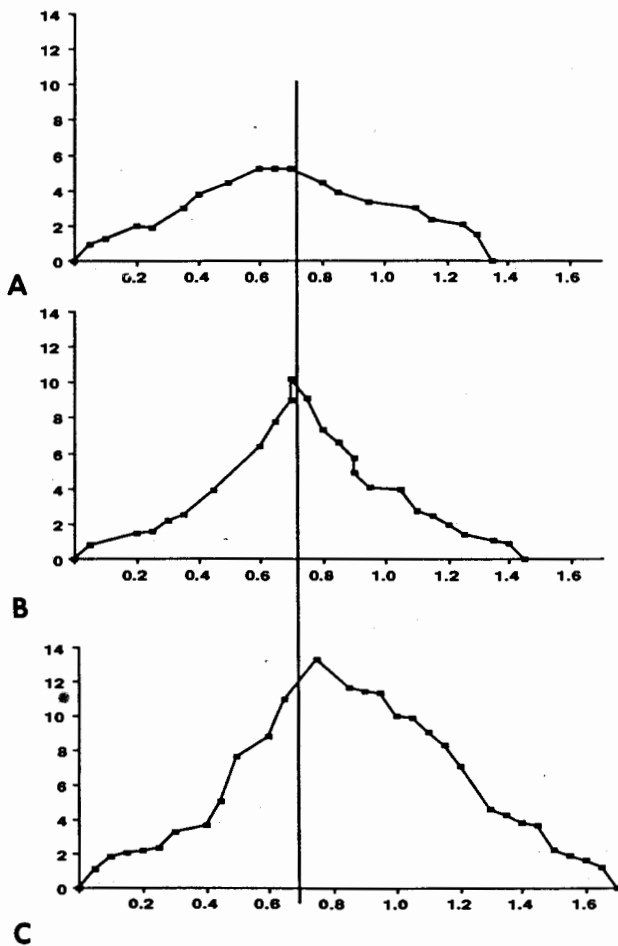


Fig 9. Timing (x-axis; in milliseconds) of peak glottal opening (y-axis; area in square millimeters) at three levels of airflow: A) 150, B) 250, and C) 400 mL/s.

exists at this point in the cycle. This hypothesis is supported by the collapsible tube model of phonation as described by Berke et al.⁷ At low flow rates, a higher resistance system exists when the subglottis and glottis are collapsed, while high flow results in a distended glottis and a lower resistance to airflow. The changes in the area of the subglottic vault are

seen in the regions of the negative pressure differential versus flow of the collapsible tube model.

The findings in this experiment contradicted those of Tully et al.,⁸ who studied the relationship between thyroarytenoid activity and laryngeal resistance. They reported no increase in "glottal aperture" with increasing flow. It is not clear how the glottal aperture was assessed in that experiment, and therefore it is difficult to determine the cause of the discrepancy.

Another part of the explanation of the increased glottal area integral with increasing airflow is provided by Fant,⁹ who hypothesized that relatively constant subglottic pressure should produce constant exit jet velocity despite increasing airflow. From Ohm's law of flow it follows that $Q = A \times f \times V$, where flow through the glottis (Q) is equal to the product of the area integral of the glottis (A), the frequency of vocal fold vibration (f), and the velocity of flow (V). Therefore, if flow increases and exit jet velocity is constant, the area integral increases.

Also, a careful analysis of the glottal area waveforms suggested that the peak glottal area occurs at a similar time relative to the initiation of glottal opening, regardless of the absolute value of airflow (Fig 9). The enlarged subglottic vault imparts more energy for opening the vocal folds, not only with a greater peak area, but also with greater displacement velocity.

In the future, our laboratory plans to extend this work by measuring the effect of increasing laryngeal resistance on glottal area by altering laryngeal nerve stimulation at constant airflow rates.

In conclusion, glottal area increased with increasing airflow, both when it was measured as peak area and when an integral was calculated over the area versus time curve. This study demonstrates the feasibility and power of recently developed techniques for the objective study of laryngeal vibration.

REFERENCES

1. D'Antonio L, Netsell R, Lotz W. Clinical aerodynamics for the evaluation and management of voice disorders. *Am J Otolaryngol* 1984;5:397-403.
2. Smith ME, Green DC, Berke GS. Pressure-flow relationships during phonation in the canine larynx. *J Voice* 1991;5:10-7.
3. Sercarz JA, Berke GS, Arnstein D, Gerratt B, Natividad M. A new technique for quantitative measurement of laryngeal videostroboscopic images. *Arch Otolaryngol Head Neck Surg* 1991;117:871-9.
4. Berke GS, Moore DM, Hanson DG, Hantke DR, Gerratt BR, Burstein F. Laryngeal modeling: theoretical, in vitro, in vivo. *Laryngoscope* 1987;97:871-81.
5. Berke GS, Trapp TK, Gerratt BR, Hanson DG, Natividad M. Videostroboscopic images associated with photoelectric measures in an in vivo canine model. *J Acoust Soc Am* 1988;85:1789-93.
6. Hayden EH, Koike Y. A data processing scheme for frame by frame film analysis. *Folia Phoniatr (Basel)* 1972;24:169-81.
7. Berke GS, Green DG, Smith ME, et al. Experimental evidence in the in vivo canine for the collapsible tube model of phonation. *J Acoust Soc Am* 1991;89:1358-63.
8. Tully A, Brancatisano A, Loring SH, Engel LA. Relationship between thyroarytenoid activity and laryngeal resistance. *J Appl Physiol* 1990;68:1988-96.
9. Fant G. Acoustic theory of speech production. The Hague, the Netherlands: Mouton and Co, 1960:247-89.